Title

Formation of cysts by alveolar type II cells in three-dimensional culture reveals a novel mechanism for epithelial morphogenesis.

Journal

Molecular biology of the cell, 18(5)

ISSN

1059-1524

Authors

Yu, Wei
Fang, Xiaohui
Ewald, Andrew
et al.

Publication Date

2007-05-01

Peer reviewed

Molecular Biology of the Cell
Vol. 18, 1693–1700, May 2007

Formation of Cysts by Alveolar Type II Cells in Three-dimensional Culture Reveals a Novel Mechanism for Epithelial Morphogenesis[V]

Wei Yu,* Xiaohui Fang,† Andrew Ewald,* Kit Wong,‡ C. Anthony Hunt,§ Zena Werb,* Michael A. Matthay,† and Keith Mostov*

Departments of *Anatomy, ‡Cellular and Molecular Pharmacology, and §Biopharmaceutical Sciences and Pharmaceutical Chemistry, and †Cardiovascular Research Institute, University of California, San Francisco, San Francisco, CA 94143

Submitted November 30, 2006; Revised January 26, 2007; Accepted February 20, 2007
Monitoring Editor: Asma Nusrat

Many organs consist of a hollow cavity surrounded by a monolayer of epithelial cells. Despite their common structure, such organs form by diverse morphogenetic processes. Three-dimensional culture systems have been useful in analyzing the events. Most processes require a combination of cell proliferation and cell death to produce a hollow cavity. Here, we describe a new three-dimensional culture system in which primary human lung alveolar type II cells formed hollow epithelial cysts by a novel process. Individual cells moved, collided, and formed alveolar-like cysts without appreciable proliferation or apoptosis. The alveolar-like cysts consisted of a polarized monolayer of differentiated alveolar type II cells, which secreted surfactant into the central lumen. Blockage of β1 integrin did not alter cell movement or collision, but it greatly reduced adhesion of cells after collision and subsequent formation of alveolar-like cysts. Treatment of preformed alveolar-like cysts with forskolin increased their diameter, possibly due to stimulation of fluid secretion into the lumen. We conclude that epithelial differentiation and cyst formation can occur without appreciable proliferation or apoptosis.

INTRODUCTION

Most internal epithelial organs consist of a monolayer of polarized epithelial cells lining a central cavity (Hogan and Kolodziej, 2002; O'Brien *et al*., 2002; Lubarsky and Krasnow, 2003). In the simplest cases, cavity shape can be roughly spherical, forming alveoli, acini, or cysts. Alternatively, the cavity can be stretched into a tube or branching tubular tree, although topologically these structures are related to hollow spheres. Such hollow structures are known to develop in vivo by a variety of pathways, which, at least superficially, seem quite different. We aim to understand the mechanisms of formation of these structures as well as the underlying principles that may emerge from studying the seemingly diverse processes of their formation.

The cellular and molecular mechanisms of epithelial morphogenesis have been extensively studied using epithelial cells grown in three-dimensional (3D) culture systems by using thick gels of extracellular matrix material (ECM), such as type I collagen or Matrigel (an extract of the basement membrane-like ECM secreted by the Engelbreth–Holm–Swarm tumor). When a single cell suspension of Madin-Darby canine kidney (MDCK) cells is plated in collagen gel at low density, the cells proliferate and over ~8 d they produce largely clonal cysts made up of a monolayer of well-polarized cells surrounding a central lumen (O'Brien *et al*., 2001; Yu *et al*., 2005). The cysts are fairly uniform in size. The formation process requires apoptosis of some cells in the cyst interior. If apoptosis is prevented by overexpression of Bcl-2, cells abnormally remain in the cyst center (Lin *et al*., 1999). Several mammary cell lines also form cysts when grown in 3D ECM gels. For example, MCF10A cells are incompletely polarized, lacking tight junctions between cells (Debnath and Brugge, 2005; Underwood *et al*., 2006). Nevertheless, they form hollow cysts lined by a monolayer of cells. Formation and maintenance of the cell-free lumen depend on a balance between cell proliferation and cell death (Debnath *et al*., 2002; Mills *et al*., 2004) and on the relative location of components in the local environment of a cell (Matthay *et al*., 2002). Neither inhibition of cell death nor overproliferation of cells alone is sufficient to prevent lumen hollowing, although a combination of these perturbations can result in a lumen filling phenotype.

To explore whether similar mechanisms of cyst and lumen formation are used by epithelial cells from other organs, we analyzed epithelial morphogenesis of lung cells in 3D culture. The lung consists of an extensively branching system of airway tubes, which end in roughly spherical alveoli, where gas exchange occurs (Matthay *et al*., 2002). There are two main types of alveolar epithelial cells: type I are squamous and constitute most of the surface area, whereas type II are cuboidal. Alveolar type (AT) II cells secrete surfactant and are the progenitors of type I cells. Under most culture conditions, AT II cells tend to differentiate into type I cells. Consequently, it has so far proven difficult to maintain surfactant-producing, human AT II cells in culture.

This article was published online ahead of print in *MBC in Press* (http://www.molbiolcell.org/cgi/doi/10.1091/mbc.E06–11–1052) on March 1, 2007.

[V] The online version of this article contains supplemental material at *MBC Online* (http://www.molbiolcell.org).

Address correspondence to: Keith Mostov (keith.mostov@ucsf.edu).

To overcome the problem of maintaining differentiation of AT II cells and to study how these cells behave in 3D culture, we studied primary human AT II cells in Matrigel cultures. The cells formed hollow cysts lined by a polarized monolayer of cells; we refer to these structures as alveolar-like cysts (ALCs). They retain specific AT II properties. The cells secrete surfactant and seem well differentiated. Hence, this culture model may provide an appropriate physiological environment to study pulmonary alveolar function. Unlike MDCK cell cysts, formation of ALCs does not involve appreciable proliferation or apoptosis. Rather, the ALCs form by cell aggregation and rearrangement. Remarkably, even though MDCK and AT II cells form epithelial structures by very different mechanisms, the results, hollow cysts lined by a polarized monolayer, are quite similar. This similarity suggests the existence of common principles of epithelial morphogenesis, despite apparent differences in mechanism.

MATERIALS AND METHODS

Isolation of Human Primary Type II Alveolar Cells

AT II cells were isolated from cadaveric human lungs that were declined by the Northern California Transplant Donor Network (Oakland, CA). We selected the lobe that had no obvious consolidation or hemorrhage by gross inspection. Previous studies indicate that these lungs are generally in a relatively normal condition physiologically and pathologically. The isolation method was described in detail in a previous report (Fang *et al*., 2006). Briefly, cells were isolated after the lungs had been preserved for 4–8 h at 4°C. The pulmonary artery was perfused with a 37°C phosphate-buffered saline (PBS) solution, and the distal air spaces were lavaged 10 times with warmed Ca^{2+}- and Mg^{2+}-free PBS solution (0.5 mM EGTA and 0.5 mM EDTA). Next, a solution of 13 U/ml elastase in Ca^{2+}- and Mg^{2+}-free Hanks' balanced salt solution was instilled into the distal air spaces by using segmental bronchial intubation. After 45 min of digestion, the lobe was minced finely in the presence of fetal bovine serum (FBS) and 500 μg/ml DNase. The cell-rich fraction was filtered sequentially through one and then two layers of gauze, followed by 150-μm and then 30-μm nylon mesh. The filtrate was layered onto a discontinuous Percoll density gradient, 1.04–1.09 g/ml, and centrifuged at 400 $\times$ *g* (1500 rpm) for 20 min. The top band, containing a mixture of type II pneumocytes and alveolar macrophages, was collected and centrifuged at 800 rpm for 10 min. The pellet was washed and resuspended in Ca^{2+}- and Mg^{2+}-free PBS containing 5% FBS. The cells were then incubated under constant mixing for 40 min at 4°C with magnetic beads coated with anti-CD-14 antibodies. The beads were then isolated using a Dynal magnet (Dynal Biotech, Oslo, Norway). The remaining cell suspension was removed and incubated in human immunoglobulin G-coated tissue culture-treated Petri dishes in a humidified incubator (5% CO_2 at 37°C) for 90 min. Unattached cells were collected and counted. Cell viability was assessed by the trypan blue exclusion method. AT II cell purity was examined by Papanicolaou staining.

Cell Culture

The freshly isolated cells were cultured in Matrigel-coated chambers in minimal essential medium (MEM) supplemented with 10% FBS and 2% high growth factor Matrigel (BD Biosciences, Bedford, MA). For immunostaining, cells were plated on coverglass-bottomed chambers (Nalge Nunc International, Naperville, IL). For electron microscopy, cells were grown on filters (Corning Life Sciences, Acton, MA). For live cell imaging, tissue culture plates (BD Biosciences Discovery Labware, Bedford, MA) were used. The cells were cultured for 5 d; the medium was changed on the third day. For immunofluorescence staining and electron microscopy examination, cells were plated at a density of 25 $\times$ 10^4 cells/cm^2.

For MDCK culture in Matrigel, MDCK cells in single cell suspension were grown on Matrigel-coated chamber in medium containing 2% Matrigel (Martin-Belmonte *et al*., 2007). The cell density was maintained at 0.25–1 $\times$ 10^4 cells/cm^2.

Antibodies and Reagents

The primary reagent antibodies were rabbit anti-pro-SP-C (Chemicon International, Temecula, CA), mouse anti-*cis*-Golgi enzyme GM130 (BD Biosciences Transduction Laboratories, Lexington, KY), rabbit anti-β-catenin (H-102) (Santa Cruz Biotechnology, Santa Cruz, CA), rat anti-zonula occludens (ZO)-1 (R40-76; a gift from Dr. Bruce Stevenson, University of Alberta, Edmonton, Alberta, Canada), mouse anti-Ki67 (MIB-1; (Zymed Laboratories, South San Francisco, CA), and rabbit anti-cleaved caspase 3 (Asp175; Cell Signal Technology, Danvers, MA). Anti-β1 integrin antibody TS2/16 was an ascites from American Type Culture Collection (Manassas, VA). LysoTracker Green DND-26 probe was from Invitrogen (Carlsbad, CA). The secondary antibodies were anti-mouse Alexa Fluor 488, anti-rabbit 555, and anti-rat 488 (Invitrogen). Actin filaments were stained with Alexa Fluor 546-phalloidin (Invitrogen). Nuclei were stained with Hoechst. AIIB2, a function-blocking rat monoclonal anti-β1 integrin antibody was a gift from Dr. Caroline Damsky (Departments of Stomatology and Anatomy, University of California, San Francisco, San Francisco, CA).

Immunofluorescence Staining

Cell samples were quickly rinsed twice with warm PBS and then fixed for 30 min with 4% paraformaldehyde. After sufficient washing, cells were blocked for 30 min with 0.7% gelatin in PBS/0.1% saponin, and then they were incubated in primary antibodies at 4°C for overnight. After washing, cells were incubated in Alexa Fluor-conjugated secondary antibodies for 1 h at room temperature. Samples were kept in PBS after washing and observed with a Zeiss 510 LSM confocal laser microscope. Images were analyzed with Adobe Photoshop software (Adobe Systems, Mountain View, CA).

Time-Lapse Images

Cells were grown in Matrigel-coated 24-well plates as described above and observed using a Zeiss Axiovert S-100 microscope (Carl Zeiss, Thornwood, NY). Time-lapse movies were recorded beginning 8 h after plating and ending after 137 h of culture. We used a 10$\times$ A-Plan objective lens on a Cohu high-performance charge-coupled device camera. Light exposure was regulated by a Ludl shutter and controller, which also controlled the Ludl x-y-z–motorized stage. Temperature and carbon dioxide were held at 37°C and 5%, respectively, by using a CTI Controller 3700 and Temperature Control 37.2 combination (Carl Zeiss). Images were acquired every 15 min at each of the 24 positions by using a custom macro implemented in OpenLab 4.0.2 (Improvision, Lexington, MA). AIIB2 was added 5 h after plating (3 h before the first image was recorded). Forskolin was added after 72 h of culture. Images were recorded using OpenLab LIFF series (Improvision) and compiled into QuickTime movies. Cell movement was analyzed with MetaMorph software (Molecular Devices, Sunnyvale, CA).

Transmission Electron Microscopy

Samples were fixed with 2% glutaraldehyde, 0.8% paraformaldehyde, and 0.1 M cacodylate buffered to pH 7.4. After washing, cells were stained with osmium and imidazole, dehydrated in graded concentrations of ethanol, and then embedded in Epon epoxy resin. Ultrathin sections were examined using a transmission electron microscope (Philips Technai 10; FEI, Hillsboro, OR).

RESULTS

Primary Human Alveolar Type II Cells Form Multicellular Structures in Matrigel

To establish a system for ALC formation, we cultured AT II cells by using a variety of collagen I and Matrigel conditions and compared the results. We found that the following approach provided reproducible cysts. Freshly isolated cells were plated at 1–25 $\times$ 10^4 cells/cm^2 on top of thin layer of 100% Matrigel with an overlay of MEM containing 2% Matrigel, as described in *Materials and Methods*. After 4–5 d of culture, multicellular ALCs had formed. Their final diameter depended on initial cell density, increasing monotonically with plated density (Figure 1, A–F). As shown in Figure 1, A–F, at 1 $\times$ 10^4 cells/cm^2, the ALC were ~25 μm in diameter, whereas at 25 $\times$ 10^4 cells/cm^2, the ALC were much larger, averaging ~62 μm in diameter (see Supplemental Material, Video 1).

To confirm that the ALC contained AT II cells, we incubated them with LysoTracker Green DND-26, a fluorescent dye that accumulates selectively in lamellar bodies in human primary AT II cells (Figure 1, G and I) (Fang *et al*., 2006). Green vesicles were found in all cells. Furthermore, the majority of vesicles were distributed between the nucleus and luminal surface. Surfactant-C is a specific protein secreted by AT II cells. To provide further evidence that the cells were AT II, we stained for prosurfactant-C (proSP-C) by immunofluorescent staining (Figure 1, J–L; red is proSP-C, green is actin stained with phalloidin). Most cells were proSP-C positive, further confirming that ALCs were made up of AT II cells. As a positive control, human lung

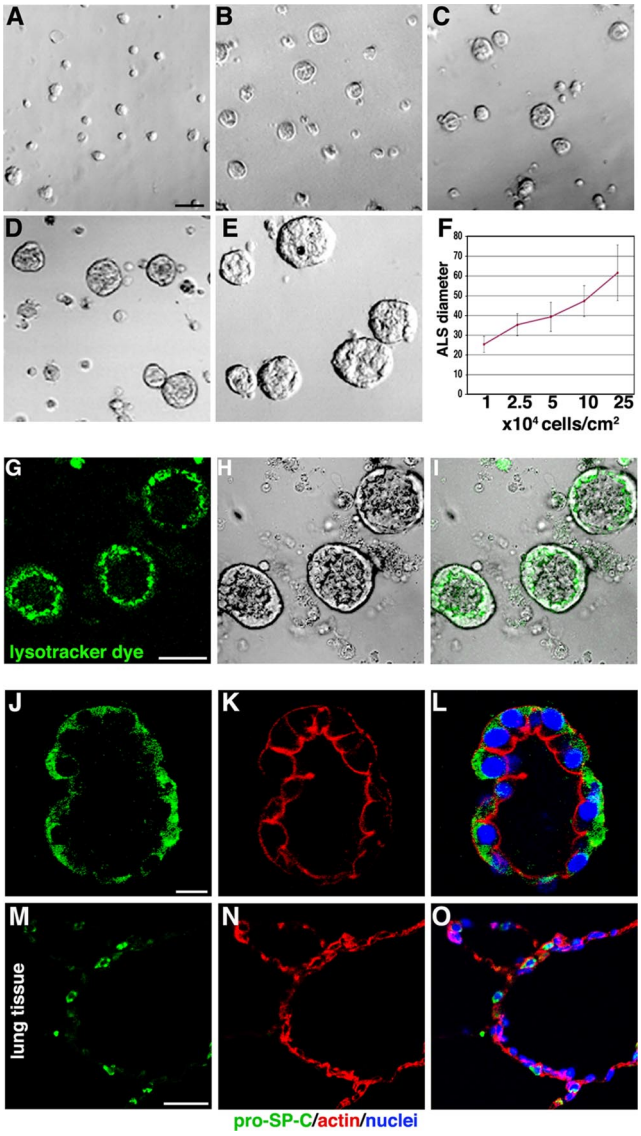

Figure 1. AT II cells form ALCs in Matrigel culture. (A–E) Phase-contrast pictures after 4 d in 2% Matrigel cultures; cells were initially plated at 1, 2.5, 5, 10, and 25 × 10^4 cells/cm^2. (F) Final ALC size was dependent on initial cell density. (G–O) Evidence that ALCs were composed of AT II cells. (G) Confocal images show ALCs stained with LysoTracker green DND-26, a fluorescent dye that accumulates in lamellar bodies. (H) Phase-contrast image of same field as in G. (I) G and H merged. (J) Green immunostaining shows proSP-C. (K) Red shows actin stained with phalloidin. (L) J and K merged. (M and N) Cryosection of human adult lung tissue was used as positive control for proSP-C (M) and phalloidin (N) staining. (O) M and N merged. Bars, 50 μm (A–E, G–I, and M–O) and 10 μm (J–L).

tissue sections were stained with proSP-C antibody. Several positive cells were observed in alveoli (Figure 1, M–O).

ALCs Are Polarized

We next examined the structure and polarity of ALC cells in detail. Fluorescence immunostaining revealed that the ALC consisted of a layer of cuboidal-shaped epithelial cells (Figure 2, A–B′) oriented around a central lumen. The tight junction marker ZO-1 (A and A′, green) was observed at the tips of cell–cell contacts facing the lumen. The basolateral

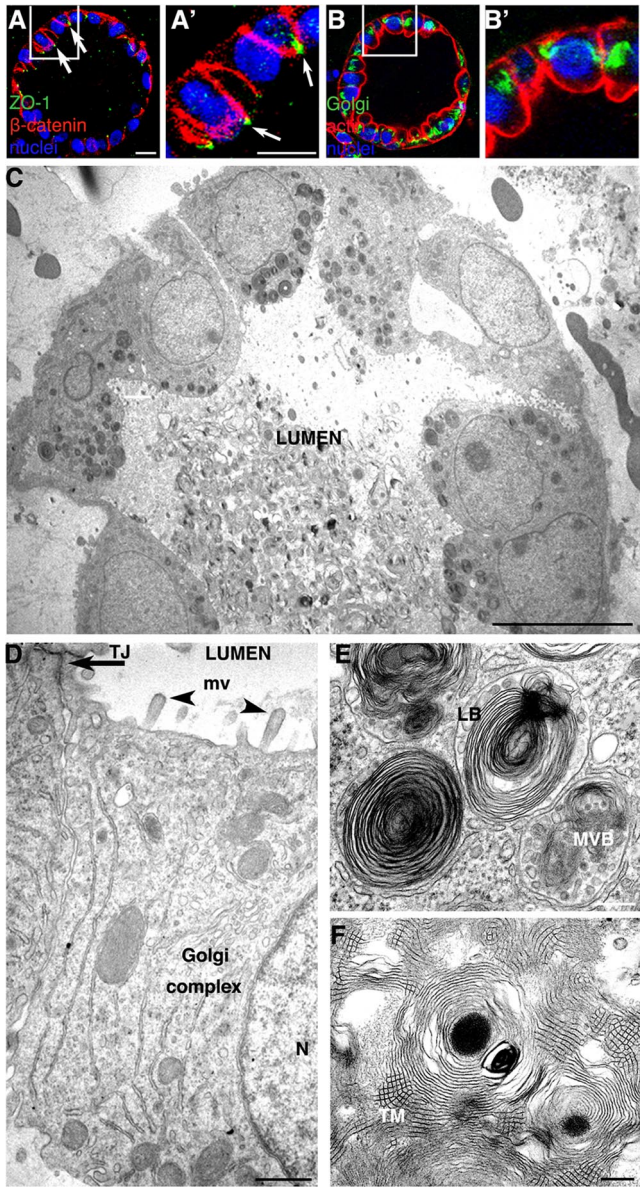

Figure 2. ALCs are well polarized. (A) Confocal micrographs of 4-d ALCs showed the basolateral marker β-catenin stained red, and the tight junction marker ZO-1 stained green. Note that ZO-1 staining was observed at cell–cell contacts facing the lumen (white arrow). (B) ALCs stained green for the Golgi marker GM130 and red for actin. GM130 was located laterally, whereas actin was localized at all plasma membranes, yet enriched at the luminal surface. A′ and B′ represent high magnification of regions indicated in A and B, respectively. (C) Electron micrographs showed cuboidal cells containing lamellar bodies; the lumen was filled with secreted lamellar bodies. (D–F) Shown is evidence of epithelial polarity and typical AT II characteristics, including numerous microvilli (arrowheads) facing the luminal surface and a tight junction structure (arrow) that was evident at cell–cell contacts near the lumen (D). The Golgi complex was between the nucleus (N) and a lateral surface. (E) Membrane-bounded LB and MVB were evident. Lamellar body contents that have been secreted from AT II cells were seen rearranged into a tubular myelin (TM) structure, which is a unique, secreted form a of surfactant protein having a lattice-like structure (F). Bars, 10 μm (A–C), 1 μm (D), and 200 nm (E and F).

protein marker, β-catenin was localized at the basolateral plasma membrane (Figure 2, A and A′, red). The Golgi

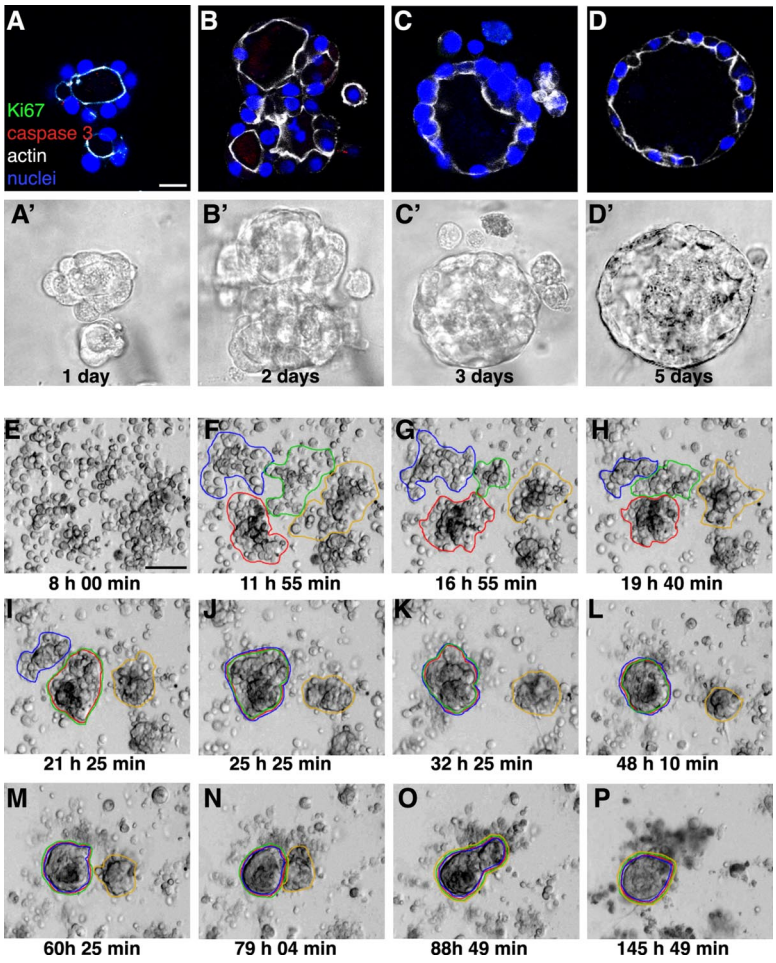

Figure 3. Confocal images show cell aggregation contributes to ALC formation. AT II cells cultured for 1, 2, 3, or 5 d (A–D, respectively) in Matrigel were stained with Ki67 (green), cleaved caspase 3 (red), actin (white), and nuclei (blue). (A′–D′) Phase-contrast images corresponding to A–D. (E–P) Shown are selected phase-contrast, time-lapse images of live cells taken 8–137 h (times indicated in each frame) after plating in Matrigel culture. (F–I) By 24 h, cells had aggregated into small clusters. (I–P) The multicellular structures in F–I aggregated further and finally became a structure having a single lumen. See Supplemental Material, Video 2, right panel. Bars, 10 μm (A–D′) and 50 μm (E–P).

complex (B and B′, green) was located lateral to the nucleus (blue), and actin (B and B′, stained red with phalloidin) was observed at all plasma membrane surfaces, but especially enriched underneath the apical cell surface.

Thin-section electron microscopy images were consistent with the preceding results: the ALCs were made up of cuboidal cells surrounding a central lumen (Figure 2C). Cells were ~10 μm/side and were polarized with their microvilli facing the lumen. Structures resembling intracellular junctional complexes were near the lumen. The Golgi complex was frequently observed between the nucleus and the lateral membrane (Figure 2D). Two types of specialized structures, characteristic of AT II cells, were observed (Figure 2E). First, membrane-bound lamellar bodies (LB) having a mean diameter of ~1 μm often accumulated between the apical surface and nuclei. Second, multivesicular bodies (MVB) were observed. They are organelles in which small vesicles are contained within the lumen of a larger vesicle. The central lumens of the ALCs were filled with secreted lamellar bodies (Figure 2C). Among these lamellar bodies, tubular myelin, a unique square lattice structure (~30–50 nm/side), was often observed (Figure 2F).

Cell Aggregation Contributes to ALC Formation

How do AT II cells grown in Matrigel form polarized ALCs that have a central lumen? To answer this question, we first looked for evidence of cell proliferation after different culture intervals by immunostaining with Ki67, which marks a nuclear antigen that is expressed in the late G_1, S, M, and G_2 phases of the cell cycle. Next, we tested for evidence of apoptosis by immunostaining for cleaved caspase 3. The method detects the 17-kDa fragment of activated caspase 3, a marker of apoptotic cell death. (Figure 3, A–D, A′–D′ show corresponding phase-contrast images of the same fields.) Neither Ki67-positive cells nor caspase 3-positive cells were detected at any of the investigated times, including after 1, 2, 3, and 5 d of culture. MDCK cysts grown in the same condition as AT II cells serve as a positive control for these two antibodies (Figure 4, D–F). These results indicated that ALC formation does not involve any significant cell proliferation or caspase 3-dependent apoptosis. These finding were further confirmed by treatment with ZVAD, a general caspase inhibitor, and aphidicolin, an inhibitor of DNA polymerase. Neither ZVAD at concentrations of 2–200 μM or aphidilocin at concentrations of 2–100 μM had a detectable effect on ALC formation (our unpublished data). In contrast, both ZVAD and aphidicolin at 10 μm had effect on MDCK cells during cyst formation (our unpublished data). Given that ALC diameter depends on initial cell density, we hypothesized that aggregation of nonproliferating cells contributes to ALC formation. To test this idea, we recorded time-lapse images as described above. Selected stills from one such movie are shown in Figure 3, E–P. The complete video is available in Supplemental Material, Video 2 (right panel). After 8 h of culture, the system consisted largely of individual cells (E). Cells moved, collided, and attached to

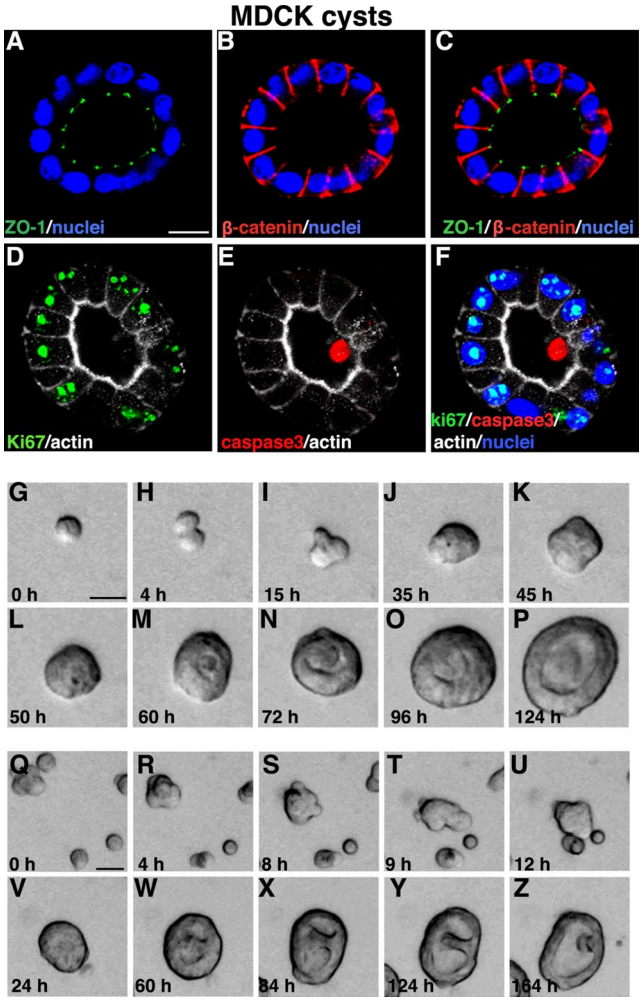

Figure 4. MDCK cells form cysts in Matrigel. (A–C) Confocal images of 5-d-old MDCK cysts grown in 2% Matrigel showed the basolateral marker β-catenin stained red, and the tight junction marker ZO-1 stained green. Note that ZO-1 staining was observed at cell–cell contacts facing the lumen. (D–F) Immunostaining with Ki67 (green in D and cyan in F when merged with nuclei in blue) and cleaved caspase 3 (red in E and F) in MDCK cysts. (G–P) Representative live images of a single MDCK cell, cultured in Matrigel for 5 d, generating a clonal cyst. (Q–Z) show still frames of live images of multiple individual MDCK cells aggregating and proliferating to form one cyst. Also see Supplemental Material, Video 3. Bars, 10 μm (A–F) and 20 μm (G–Z).

each other. Aggregates formed (e.g., F and G). Later, small aggregates had coalesced to form larger aggregates (H–L): later still, a few large aggregates were seen along with several remaining individual cells (M–P). By 24 h, well-organized structures were evident. Thereafter, further aggregation and rearrangement produced ALCs. The images in Figure 3, E–P, were from cells plated at a high density. We also analyzed cultures plated at lower densities (our unpublished data). The same pattern of cell movement and aggregation was observed, although the aggregates were proportionately smaller when the cell density was lower.

We quantified cell movement for 4–6 h by tracing individual cell paths (n = 61) after plating at 25×10^4 cells/cm^2. Cell movement averaged 1.8 μm/15 min. Aggregation always followed collision: within the first 6 h, ~60% of individual cells adhered to neighbors.

We also examined whether increasing Matrigel concentration has effect on ALC formation. We compared AT II cells grown with either 2 or 10% Matrigel overlaying the cells, which were always plated on a base of 100% Matrigel. We collected phase-contrast time-lapse images, and we analyzed the speed of cell movement in the first few hours in culture. We found cells moved slower in 10% Matrigel culture than in 2% Matrigel (1.21 μm/15 min in 10% Matrigel versus 1.70 μm/15min in 2% Matrigel), and they formed smaller cysts (~48 μm in diameter) in 10% Matrigel than in 2% Matrigel (~62 μm in diameter). These findings are consistent with our hypothesis that AT II cells form ALCs by aggregation.

MDCK Cells Form Cysts in Matrigel

MDCK cells form well polarized cysts in collagen or Matrigel culture. MDCK cysts in 2% Matrigel consist of a well-polarized monolayer, with the tight junction marker ZO-1 (Figure 4, A and C, green) located at the tips of cell–cell contacts facing the lumen. The basolateral protein marker β-catenin was localized at the basolateral plasma membrane (Figure 4, B and C, red). During MDCK cyst formation, cell proliferation as well as apoptosis in the central lumen was observed as revealed by immunostaining with Ki67 (green in Figure 4, D and F) and cleaved caspase 3 (red in Figure 4, E and F). By analysis of phase-contrast time-lapse images, we further found that MDCK cells form clonal cysts almost entirely by cell proliferation when plated at very low density. However, when cells are plated at high density, both proliferation and aggregation can occur concurrently. Figure 4, G–Z, shows examples of these two types of mechanism of MDCK cyst formation: cell proliferation alone (G–P, and Supplemental Material, Video 3, left panel) and cell proliferation combined with aggregation (Figure 4, Q–Z, and Supplemental Material, Video 3, right panel).

β1 Integrin Is Required for Cell Aggregation, not Cell Movement

The β1-containing integrins (α1β1, α3β1, and α5β1) have been found in human lung alveolar cells (Koukoulis *et al.*, 1991). We observed that β1 integrin was expressed at the ALC basolateral surface (Figure 5, A and B). To determine whether β1 integrin was involved in ALC formation, we applied AIIB2, a function-blocking antibody against β1 integrin, to cells 5 h after plating, after they adhered to ECM (adding AIIB2 earlier prevented adherence to the Matrigel). We found that cells were still able to move: their speed averaged 1.7 μm/15 min (n = 68) (Figure 5C and Supplemental Material, Video 2, left panel), and frequent collisions occurred. No significant difference was observed in speed of movement between untreated and AIIB2-treated cells (Figure 5C). However, in the presence of AIIB2, only 25% of individual cells adhered to neighbors within the first 6 h (Figure D). Furthermore, the small clusters that did form failed to aggregate further (Figure 5, E–H, and Supplemental Material, Video 2, left panel). Based on these findings, we suggest that β1 integrin is required for AT II cell aggregation but not for cell movement.

Activation of cAMP Results in Larger Lumens and Thinner Cells

cAMP-regulated fluid transport plays an important role in pulmonary alveolar function. Activation of cAMP production by forskolin increases fluid transport (Matalon *et al.*, 2002; Matthay *et al.*, 2002). We hypothesized that forskolin treatment would increase fluid transport across the AT II cells, thereby increasing the diameter of the central lumen.

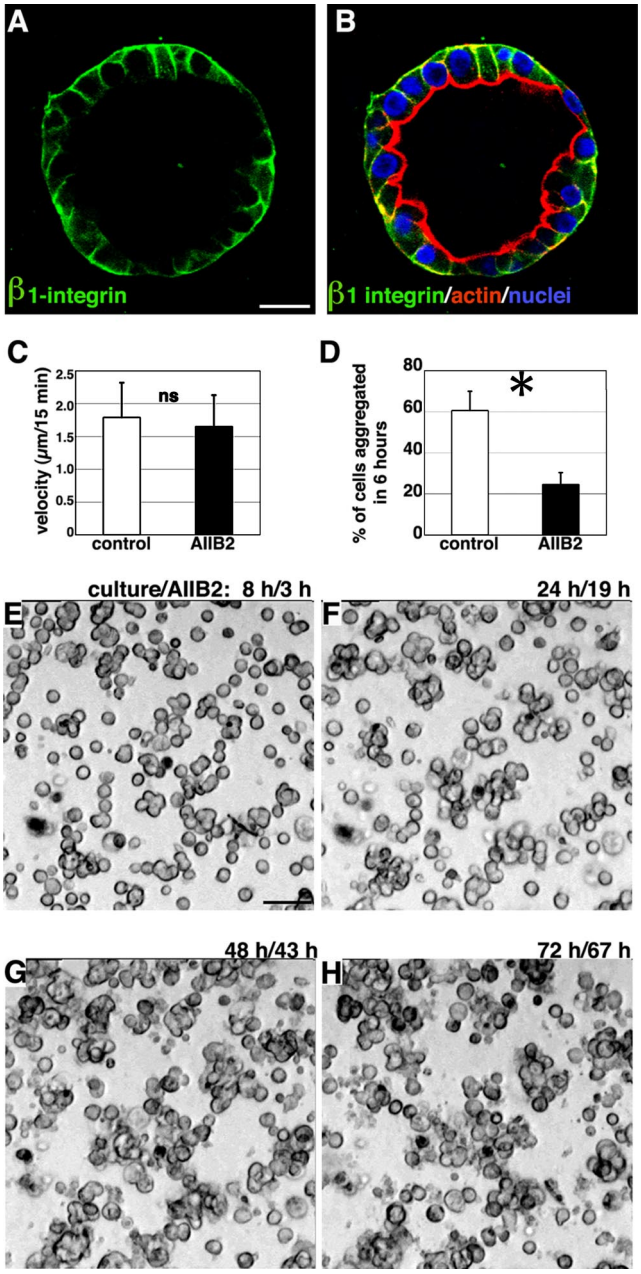

Figure 5. β1-Integrin is required for cell aggregation. (A) Green immunofluorescent staining of β1-integrin revealed that it was localized at the ALC basolateral surface. (B) The green staining in A is shown merged with red actin staining and blue nuclear staining. (C) Individual AT II cells in Matrigel in the presence of AIIB2 moved at an average speed of 1.7 μm/15 min. Control cells moved at 1.8 μm/15 min. ns, no significant difference between the two means. (D) Sixty one percent of individual cells adhered to other cells during the 6-h interval starting from 8 h after plating. In the presence of AIIB2, only 25% of cells adhered; the majority remained as individual cells; *, $p < 0.01$ (Student's *t* test). (E–H) Representative time-lapse images of AIIB2-treated cells. Note that even after 3-d culture, cells only formed small clusters: many remained single. Bars, 10 μm (A and B) and 50 μm (E–H).

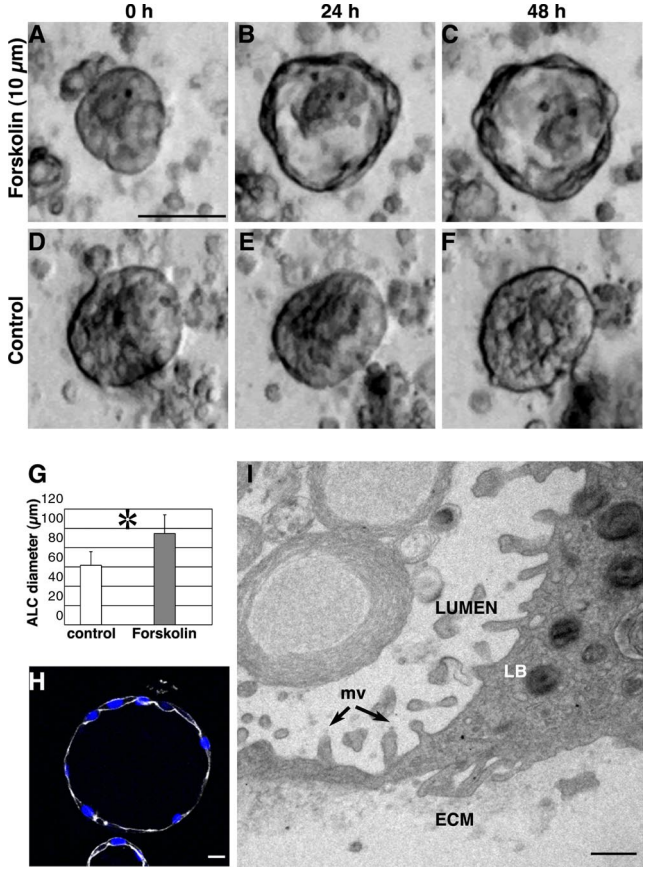

Figure 6. Forskolin treatment expands ALCs. Addition of 10 μM forskolin to ALCs after 3 d in culture increased ALC size within 24 h: the central lumen expanded and became more evident. (A–C) Phase-contrast images of cysts 0, 24, and 48 h after forskolin addition. (D–F) Over the same time interval, control ALCs remained the same diameter. (G) Forty-eight hours after forskolin treatment average ALC diameter increased from 60 μm (control) to 95 μm. *, $p < 0.01$. (H) This confocal image shows forskolin-treated ALCs stained green for Ki67, red for activated caspase 3, white for actin, and blue for nuclei; no significant Ki67- or caspase 3-positive cells were seen, whereas cells became thinner. (I) Transmission electron micrograph showing a portion of a cell within an ALC that had been exposed to forskolin for 24 h. The cell still contained LB. Microvilli (mv) were observed at the luminal surface, and some parts of the cell were very thin: <1 μm distance from apical to basolateral surface. Bars, 50 μm (A–F), 10 μm (H), and 1 μm (I).

To test this idea, we added forskolin to 3- to 4-d-old cell cultures and compared ALC diameters at different initial cell densities. Over a 24-h period, all ALCs expanded. Figure 6, A–C, shows that at 25×10^4 cells/cm^2, ALC size increased 60% (to an average diameter of 95 μm, as shown in Figure 6G); the untreated ALCs did not change size (Figure 6, D–F). Cyst expansion was accompanied by dramatic fluid filling of the lumen (see Supplemental Material, Video 4, right panel). To further confirm that the size increase was not due to cell proliferation, we stained with Ki67 and an antibody to activated caspase 3 (Figure 6H). We found no positive cells: the forskolin induced size change was not the result of increased cell proliferation. We also observed that the cells in forskolin-treated ALCs were much flatter (squamous) than were those in control ALCs. Electron micrographs (Figure 6I) showed that some cell heights were <0.5 μm, yet the cells still contained lamellar bodies and had microvilli at their apical surfaces. These findings suggest that AT II cells did not differentiate to type I cells during the span of these experiments, even though cell shape changed with forskolin exposure.

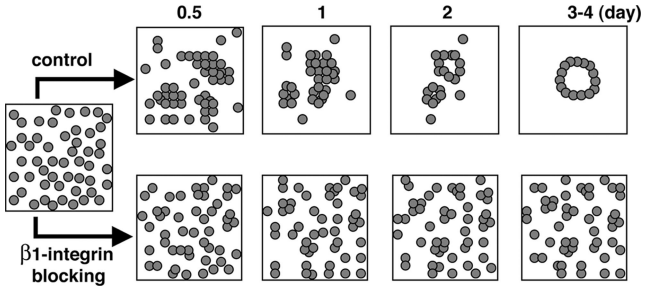

Figure 7. Schematic illustrates events during ALC formation and the blocking effect of β1-integrin. AT II cells in Matrigel begin aggregating 0.5 d after plating: cells formed small clusters by day 1. Further aggregation followed, and by 3–4 d polarized ALCs had formed. Blocking β1-integrin inhibited cell aggregation. Cells frequently collided with neighboring cells but largely failed to adhere.

DISCUSSION

Primary human AT II cells in 3D Matrigel form ALCs made up of a monolayer of epithelial cells surrounding a central lumen. The cells are highly polarized and exhibit properties characteristic of differentiated AT II cells: surfactant and tubular myelin are produced. As with many other epithelial cell types, 3D culture of AT II cells is optimal for preservation of the differentiated phenotype. The structures formed closely resemble those seen in vivo.

In the most thoroughly studied 3D culture system, MDCK cells at 2×10^4 cells/ml individual cells proliferate and produce largely clonal cysts (Pollack *et al*., 1998; O'Brien *et al*., 2001; Yu *et al*., 2005). Their final size is relatively constant. In contrast, under identical conditions, AT II cells do not proliferate significantly. Rather, as the diagrammed in Figure 7, they migrate, collide, and aggregate to form ALCs. Consequently, the ultimate ALC size is roughly proportional to initial density: plating at a higher cell density leads to more collisions and larger aggregates. Under the same conditions, some MDCK cells within cysts undergo apoptosis. It occurs primarily in the lumen and is necessary for hollow lumen formation. In contrast, we observed almost no apoptosis (or at least no activated caspase 3) at any time in ALCs. Nevertheless, the well-polarized cells formed hollow cysts with a uniform monolayer around a central lumen. In their final form, they resembled MDCK cyst grown in collagen gels. However, ALC lumen formation can occur without apoptosis and instead, must depend entirely on other processes, such as cell rearrangement.

Integrins are heterodimers of α and β subunits and are major receptors for ECM (Hynes, 1992). As stated above, single MDCK cells embedded in collagen I matrix form cysts in which apical poles of cells are oriented toward the central lumen, with basolateral poles oriented toward matrix. Inhibition of β1 integrin with AIIB2, a β1 integrin function-blocking antibody, causes inverted polarity in MDCK cysts, i.e., the apical surface faces the periphery of the cyst, whereas the basolateral surface faces the center, which lacks a lumen (Yu *et al*., 2005). Surprisingly, when we examined the involvement of β1 integrins in ALC formation, we found that its blockade abrogated ALC formation. The velocity of cell migration was not affected. Instead, cells primarily failed to adhere after collision (Figure 7), suggesting that β1 integrins play a crucial role in AT II cell–cell adhesion. Classically, integrins are most commonly thought to be involved in cell–ECM interactions (Giancotti and Ruoslahti, 1999). Some cell types are able to shift from a classical, β1 integrin-dependent migration mode to an amoeboid, β1 integrin-independent mode (Hegerfeldt *et al*., 2002; Wolf and Friedl, 2006). The observed β1 integrin-independent movement of AT II cells may be related to the latter. β1 integrins have also been shown to be involved in keratinocyte cell–cell interactions and, by inference, may play a similar role in our system (Carter *et al*., 1990; Larjava *et al*., 1990).

Treatment of ALC with forskolin, which activates AMP cyclase and increases cAMP production, lead to cyst enlargement. The cells became flatter, yet they still produced surfactant; they did not seem to differentiate into type I cells. A plausible explanation is that the increased cAMP led to fluid secretion into the lumen, which caused lumen expansion. The AT II cells may have thus been flattened by the hydrodynamic distension of the enlarged lumen. Similarly, in the fluid-filled fetal lung, increased cAMP leads to luminal fluid secretion (McCray and Welsh, 1991). Because ALCs were filled with fluid, they may have behaved like fetal lung alveoli. In contrast, in postnatal, air-filled alveoli, increased cAMP leads to fluid pumping in the opposite direction, i.e., fluid removal from the airspace.

A major finding is that unlike MDCK and MCF10A cysts, ALCs form without significant cell proliferation or apoptosis. Two seemingly very different cyst formation processes, one process mainly relying on proliferation and apoptosis, and the other relying on aggregation and rearrangement, can lead to a very similar outcome: a hollow sphere of polarized epithelial cells. Moreover, MDCK cells can form cysts either by proliferation and apoptosis alone, or by a combination of proliferation/apoptosis and aggregation, depending on the experimental conditions. This indicates that the aggregation mechanism is not unique to AT II cells but that it can be used by several different cell types and that one cell type (MDCK) can use multiple mechanisms, depending on the circumstances. The similarity of final forms suggests that common principles of organization of multicellular epithelial structures underlie seemingly diverse pathways for cyst formation. We are just beginning to explore what these principles might be (Grant *et al*., 2006). We hope that our results will encourage the search for unifying principles encompassing this diversity.

ACKNOWLEDGMENTS

We thank Sandra Huling (University of California, San Francisco [UCSF], Liver Center Core Facility) for electron micrographs. We also thank the UCSF Comprehensive Cancer Center Laboratory for Cell Analysis for access to time-lapse imaging equipment. W.Y. was supported by fellowship from the National Kidney Foundation. A.J.E. was supported by the California Breast Cancer Research Program 11FB-0015. This work was supported by National Institutes of Health grant AI-053194 (to K.M., M.M., and Z.W.). Work in M.M.'s laboratory was supported by National Heart, Lung, and Blood Institute grants HL-51854 and 51856.

REFERENCES

Carter, W. G., Wayner, E. A., Bouchard, T. S., and Kaur, P. (1990). The role of integrins alpha 2 beta 1 and alpha 3 beta 1 in cell-cell and cell-substrate adhesion of human epidermal cells. J. Cell Biol. *110*, 1387–1404.

Debnath, J., and Brugge, J. S. (2005). Modelling glandular epithelial cancers in three-dimensional cultures. Nat. Rev. Cancer *5*, 675–688.

Debnath, J., Mills, K. R., Collins, N. L., Reginato, M. J., Muthuswamy, S. K., and Brugge, J. S. (2002). The role of apoptosis in creating and maintaining luminal space within normal and oncogene-expressing mammary acini. Cell *111*, 29–40.

Fang, X., Song, Y., Hirsch, J., Galietta, J., Pedemonte, N., Zemans, R., Dolganov, G., Verkman, A., and Matthay, M. (2006). Contribution of CFTR to apical-basolateral fluid transport in cultured human alveolar epithelial type II cells. Am. J. Physiol. *290*, L242–L249.

Giancotti, F. G., and Ruoslahti, E. (1999). Integrin signaling. Science *285*, 1028–1032.

Grant, M., Mostov, K., Tlsty, T. D., and Hunt, C. A. (2006). Simulating properties of in vitro epithelial cell morphogenesis. PLoS Comput. Biol. 2, e129.

Hegerfeldt, Y., Tusch, M., Brocker, E., and Friedl, P. (2002) Collective cell movement in primary melanoma explants: plasticity of cell-cell interaction, beta1-integrin function, and migration strategies. Cancer Res. *62*, 2025–2030.

Hogan, B., and Kolodziej, P. (2002). Organogenesis: molecular mechanisms of tubulogenesis. Nat. Rev. Genet. *3*, 513–523.

Hynes, R. (1992). Integrins: versatility, modulation, and signaling in cell adhesion. Cell *69*, 11–25.

Koukoulis, G., Gould, V., Bhattacharyya, A., Gould, J., Howeedy, A., and Virtanen, I. (1991). Tenascin in normal, reactive, hyperplastic, and neoplastic tissues: biologic and pathologic implications. Hum. Pathol. *22*, 636–643.

Larjava, H., Peltonen, J., Akiyama, S., Yamada, S., Gralnick, H., Uitto, J., and Yamada, K. M. (1990). Novel function for beta 1 integrins in keratinocyte cell-cell interactions. J. Cell Biol. *110*, 803–815.

Lin, H. H., Yang, T. P., Jiang, S. T., Yang, H. Y., and Tang, M. J. (1999). Bcl-2 overexpression prevents apoptosis-induced Madin-Darby canine kidney simple epithelial cyst formation. Kidney Int. *55*, 168–178.

Lubarsky, B., and Krasnow, M. A. (2003). Tube morphogenesis. Making and shaping biological tubes. Cell *112*, 19–28.

Martin-Belmonte, F., Gassama, A., Datta, A., Yu, W., Rescher, U., Gerke, V., and Mostov, K. (2007). PTEN-mediated apical segregation of phosphoinositides controls epithelial morphogenesis through Cdc42. Cell *128*, 383–397.

Matalon, S., Lazrak, A., Jain, L., and Eaton, D. C. (2002). Biophysical properties of sodium channels in lung alveolar epithelial cells. J. Appl. Physiol. *93*, 1852–1859.

Matthay, M., Folkesson, H., and Clerici, C. (2002). Lung epithelial fluid transport and the resolution of pulmonary edema. Physiol. Rev. *82*, 569–600.

McCray, P., Jr., and Welsh, M. (1991). Developing fetal alveolar epithelial cells secrete fluid in primary culture. Am. J. Physiol. *260*, L494–L500.

Mills, K., Reginato, M., Debnath, J., Queenan, B., and Brugge, J. S. (2004). Tumor necrosis factor-related apoptosis-inducing ligand (TRAIL) is required for induction of autophagy during lumen formation in vitro. Proc. Natl. Acad. Sci. USA *101*, 3438–3443.

O'Brien, L. E., Jou, T. S., Pollack, A. L., Zhang, Q., Hansen, S. H., Yurchenco, P., and Mostov, K. E. (2001). Rac1 orientates epithelial apical polarity through effects on basolateral laminin assembly. Nat. Cell Biol. *3*, 831–838.

O'Brien, L. E., Zegers, M.M.P., and Mostov, K. E. (2002). Opinion: building epithelial architecture: insights from three-dimensional culture models. Nat. Rev. Mol. Cell Biol. *3*, 531–537.

Pollack, A. L., Runyan, R. B., and Mostov, K. E. (1998). Morphogenetic mechanisms of epithelial tubulogenesis: MDCK cell polarity is transiently rearranged without loss of cell-cell contact during scatter factor/hepatocyte growth factor-induced tubulogenesis. Dev. Biol. *204*, 64–79.

Underwood, J., Imbalzano, K., Weaver, V., Fischer, A., Imbalzano, A., and Nickerson, J. (2006). The ultrastructure of MCF-10A acini. J. Cell Physiol. *208*, 141–148.

Wolf, K., and Friedl, P. (2006). Molecular mechanisms of cancer cell invasion and plasticity. Br. J. Dermatol. *154* (suppl 1), 11–15.

Yu, W., Datta, A., Leroy, P., O'Brien, L., Mak, G., Jou, T., Matlin, K. S., Mostov, K. E., and Zegers, M. (2005). β1-integrin orients epithelial polarity via Rac 1 and laminin. Mol. Biol. Cell *16*, 433–445.